GEOPHYSICAL RESEARCH LETTERS, VOL. 25, NO. 9, PAGES 1363-1366, MAY 1, 1998

Ice nucleation processes in upper tropospheric wave-clouds observed during SUCCESS

E. J. Jensen[1], O. B. Toon[2], A. Tabazadeh[1], G. W. Sachse[3], B. E. Anderson[3], K. R. Chan[1], C. W. Twohy[4], B. Gandrud[4], S. M. Aulenbach[4], A. Heymsfield[4], J. Hallett[5], and B. Gary[6]

Abstract. We have compared in situ measurements near the leading-edges of wave-clouds observed during the SUCCESS experiment with numerical simulations. Observations of high supersaturations with respect to ice (> 50%) near the leading edge of a very cold wave cloud (T < -60°C) are approximately consistent with recent theoretical and laboratory studies suggesting that large supersaturations are required to homogeneously freeze sulfate aerosols. Also, the peak ice crystal number densities observed in this cloud (about 4 cm^{-3}) are consistent with the number densities calculated in our model. In the warmer wave-cloud ($T \simeq$ -37°C) relatively large ice number densities were observed (20–40 cm^{-3}). Our model calculations suggest that these large number densities are probably caused by activation of sulfate aerosols into liquid droplets followed by subsequent homogeneous freezing. If moderate numbers of effective heterogeneous freezing nuclei (0.5–1 cm^{-3}) had been present in either of these clouds, then the number densities of ice crystals and the peak relative humidities should have been lower than the observed values.

Introduction

Over the past few decades, several studies have shown that cirrus clouds play an important role in the earth's radiation budget and climate [e.g., Liou, 1986]. Hence, it is important to understand the processes responsible for their formation. In particular, the temperatures and humidities required for ice nucleation may control cirrus frequency. Theoretical analyses have been used to predict the ice supersaturation required for homogeneous freezing of sulfate aerosols [Sassen and Dodd, 1989; Heymsfield and Sabin, 1989; Jensen et al., 1994], and it has been suggested that this is probably the dominant ice nucleation mechanism in cirrus clouds. However, these predictions have not been extensively confirmed with atmospheric observations. Nor is it clear what role heterogeneous ice nucleation plays.

The processes responsible for cirrus cloud formation (i.e., ice nucleation and growth) are typically very difficult to study with in situ observations. Midlatitude continental cirrus clouds are usually highly structured with sporadic and localized nucleation [e.g., Sassen et al., 1989]. It is often impossible to tell what stage of evolution a sampled cloud element was in. Wave-clouds that form at the cold crests of mountain waves are ideal systems to study cloud physical processes because the wind field is laminar and well defined, and the cloud is stationary. Ice crystals nucleate at the leading (upwind) edge of the cloud, and grow as they are advected downwind. Heymsfield and Miloshevich [1993, 1995] exploited observations in wave-clouds to explore ice nucleation mechanisms at temperatures ranging from -31°C to -56°C. Although updraft velocities in wave-clouds may be larger than in typical cirrus, the wave-clouds are still useful to study cloud processes.

In this study we have combined observations from the SUCCESS mission with numerical modeling to evaluate ice nucleation processes in two wave clouds at very different temperatures (-64°C and -37°C). We will show that the observed critical humidities for ice nucleation and ice crystal number densities are consistent with calculations assuming that homogeneous freezing of sulfate aerosols is the dominant nucleation mechanism. The first section of the paper briefly summarizes the SUCCESS wave-cloud observations used in this study. Next, we describes the wave-cloud formation simulations. Finally, we compare the model results with observations and evaluate the implications for ice nucleation processes.

SUCCESS Wave-cloud Measurements

For comparison with nucleation simulations, we require measurements of peak relative humidities and ice crystal number densities at the wave-cloud leading edges. Relative humidities are calculated from the laser hygrometer water vapor measurements [Collins et al., 1995], and the meteorological measurement system (MMS) temperature measurements on board the NASA DC-8. Given the uncertainties in these measurements, the uncertainty in the derived relative humidity with respect to ice (RHI) is about 10%. During the flight on May 2, the leading edge of a wave-cloud system over Colorado was crossed several times. In this study, we will focus on the leading-edge crossings at 20:18:28 UT and 20:29 UT, when the dynamics seemed to approximately match the idealized wave-cloud model. At these times, the DC-8 flew approximately downwind into the leading-edge of the wave-cloud (20:18:28 UT crossing) and upwind out of the leading-edge (20:29 UT crossing). The measured temperature, relative humidity, and ice crystal number density are plotted versus time for the first crossing in Figure 1. The peak number densities of ice crystals larger than about 3 μm radius measured by both the counterflow virtual impactor (CVI) and the video ice particle sampler (VIPS) were about 2–7 cm^{-3}, and the peak RHI was about 150–160%. Ice

[1]NASA Ames Research Center, Moffett Field, CA
[2]University of Colorado, Boulder, CO
[3]NASA Langley Research Center, Hampton, VA
[4]National Center for Atmospheric Research, Boulder, CO
[5]Desert Research Institute, Reno, NV
[6]Jet Propulsion Laboratory, Pasadena, CA

Paper number 98GL00299.
0094-8534/98/98GL-00299$05.00

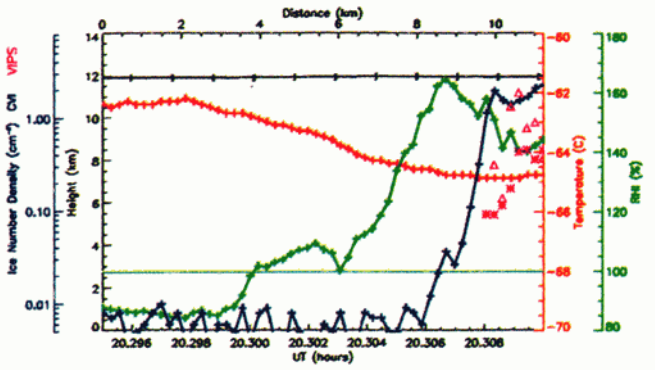

Figure 1. DC-8 measurements for the leading-edge crossing at 20:18:28 UT, May 2 are plotted versus time. At this time, the DC-8 flew downwind into the leading-edge of the wave-cloud at 11.9 km. The measured temperature (MMS), relative humidity (laser hygrometer), and ice crystal number density (CVI and VIPS) are plotted versus time. The magenta asterisks and triangles are the VIPS data from the low resolution and high resolution cameras, respectively.

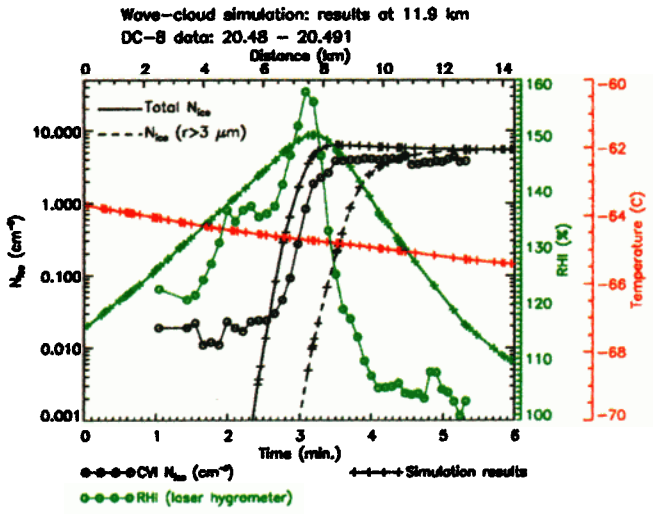

Figure 2. The model RHI, ice crystal number density, and temperature are plotted versus time at 11.9 km for the May 2 case. The total number density of ice crystals (solid black curve) and the number density of ice crystals with radii larger than about 3 μm (dashed curve) that would be detected by the CVI are shown. The DC-8 RHI and CVI data from the pass at 20:29 UT have also been plotted versus time (converted to parcel time advected by the wind) for comparison.

number densities larger than about 10 cm^{-3} were never observed in this wave-cloud.

During the wave-cloud sampling flight on April 30, we were not able to fly legs directly upwind of the cloud due to restricted air-space. However, several legs were flown along the leading edge dipping in and out of the cloud. The peak RHIs measured just upwind of this cloud were on the order of 120–130%, and the peak ice number densities indicated by the CVI ranged from 20 to 40 cm^{-3}. The actual maximum RHI may not have been detected due to the cross-wind flight path.

The temperature at the cloud leading edge for the May 2 case was about –64°C. For the April 30 case the temperature was about –37°C. The slope of the potential temperature surfaces (measured by the microwave temperature profiler (MTP)) on the upwind side of the wave crest indicated a vertical wind speed of about 1.2 m-s^{-1} for the May 2 case. This estimate approximately agrees with the vertical wind speed indicated by MMS. The vertical wind speeds indicated by MMS in the April 30 wave-cloud were much stronger (updrafts up to 5 m-s^{-1}). These vertical wind speed measurements have large uncertainties; the sensitivity of the model results to vertical wind speed is discussed below. The temperatures, humidities, ice number densities, and plausible ranges for vertical wind speeds for the two wave-cloud cases are given in Table 1.

Wave-Cloud Ice Nucleation Simulations

To simulate ice nucleation at the wave-cloud leading edges, we used a one-dimensional version of the detailed ice cloud model described by Jensen et al. [1994]. Previously, we have used this model to evaluate the sensitivity of cirrus clouds to sulfate aerosol number density, temperature, and cooling rate [Jensen and Toon, 1994]; and heterogeneous ice nuclei [Jensen and Toon, 1997]. Three particle types are included: pure sulfate solution aerosols (H_2SO_4/H_2O), activated water droplets, and ice crystals. For each particle type, 60 radius bins are included spanning the ranges 0.005 – 100 μm for sulfate aerosols and droplets, and 0.01 – 232 μm for ice crystals. For the sulfate aerosols, we assume a log-normal size distribution with $N = 100$ cm^{-3}, $r_o = 0.02$ μm, and $\sigma = 2.3$.

Tabazadeh et al. [1997] used recent laboratory data to develop new expressions for the physical quantities that control homogeneous freezing of sulfate aerosols. We have used the expressions recommended by Tabazadeh et al. to calculate aerosol freezing rates in this work. In some of the simulations, we also included heterogeneous freezing nuclei (see Jensen and Toon [1997] for details of the heterogeneous freezing calculations).

We initialized the model atmospheric temperature profiles based on SUCCESS measurements (MTP and MMS). We used an initial RHI vertical profile with a Gaussian shape peaked where the wave-cloud was observed (11.9 km). The peak RHI was initially set at just below 100%. The updraft velocity in the model oscillated sinusoidally with time; however, over the short

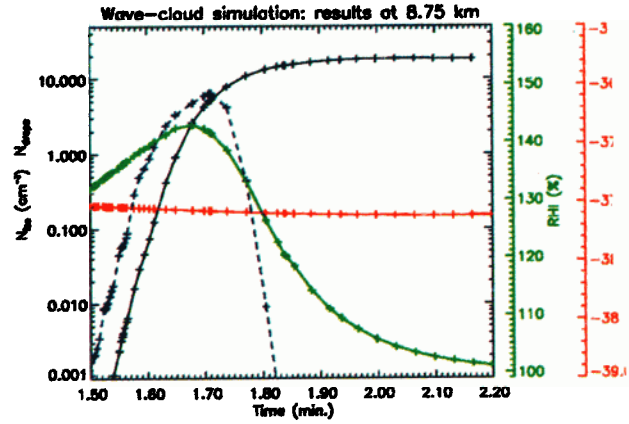

Figure 3. Same as Figure 2, but for the April 30 wave-cloud case. We also show the liquid droplet number density versus time in this case.

Table 1. Summary of SUCCESS Wave-Cloud Measurements

Date	May 2, 1996	April 30
Time (UT)	20:29:12	21:12:00
Temp	–64°C	–36.7°C
Updraft	0.8–1.6 m-s^{-1}	3–5 m-s^{-1}
Peak RHI	150–160%	≥130%
Peak Ice Conc.	2–7 cm^{-3}	20–40 cm^{-3}

time-period during which nucleation occurred, the vertical wind speed did not vary substantially.

Results

May 2, 1996 Case

We are assuming here that our 1-D model represents a column of air passing through the wave-cloud. For comparison with aircraft data, we extracte the model results versus time at the DC-8 flight level. Figure 2 shows the model RHI, ice crystal number density, and effective radius versus time at 11.9 km for the May 2 case. Ice crystals do not begin nucleating in this simulation until the RHI reaches 145–150%. In addition to the total number of ice crystals, we also show the number density of crystals with radii larger than about 3 μm that would be detected by the CVI. The crystals take about 28 seconds to grow to 3 μm, so the number of detectable crystals does not rapidly increase until just after the RHI reaches its maximum. Using the aircraft speed and ambient wind speed, we have converted the time-series data from the pass at 20:29 UT to a data series versus time as an air parcel would have been entering the leading edge and overlaid the data on Figure 2. The peak RHI and ice number density from the simulation agree reasonably well with the observed values. The observed peak RHI was about 10% larger than predicted by our model, and ice crystals were detected by the CVI further upwind that predicted by the model.

The sensitivity of the model results to key environmental conditions assumed in the model is summarized in Table 2. As discussed previously by Jensen and Toon [1994], changes in the updraft velocity can substantially change the peak ice crystal number density; whereas changes in the sulfate aerosol number density and size distribution have only moderate impact on the number of ice crystals nucleated. A reduction of the updraft speed to 0.8 m-s^{-1} reduces the peak ice crystal number density to less than 4 cm^{-3} and improves the agreement with the observations. Ice crystal growth rates are another important source of uncertainty in the model. For our baseline simulation, we assumed that the deposition coefficient (or mass accommodation coefficient) was unity. Decreasing this parameter to 0.5 results in an increase in the peak ice number density to 9.8 cm^{-3}.

The peak ice saturation in these simulations is almost entirely controlled by the assumed freezing properties of the sulfate aerosols. Changes in cooling rate or crystal growth rate do not affect the peak RHI. We have previously suggested that at temperatures below –60°C the sulfate aerosols should freeze when the RHI exceeds only about 125% (rather than about 150% indicated by our current freezing parameterization). The May 2 wave-cloud measurements suggest that the ice supersaturation required for homogeneous freezing may be as high as 160%. As indicated by the last entry in Table 1, if we use our old aerosol freezing parameterization, then not only is the peak RHI decreased to about 126%, the peak ice crystal number density is 17 cm^{-3} (much higher than the observed values).

For the rapid cooling rate and low temperature of this wave-cloud, the peak crystal number density is probably controlled exclusively by homogeneous freezing. However, heterogeneous nuclei could modify the crystal number density in wave-clouds if a substantial fraction of the sulfate aerosols contained effective heterogeneous freezing nuclei. Simulations including heterogeneous ice nuclei indicate that the number density of ice crystals generated could be reduced compared to the number generated by homogeneous freezing of pure sulfate aerosols (see Table 2). Also, if substantial numbers of effective heterogeneous ice nuclei are included, then the peak RHI at the cloud leading edge is much lower than the observed values. The consistency between the observed peak ice number densities and RHIs and the results from modeling with only homogeneous freezing suggests that relatively large numbers of effective heterogeneous ice nuclei ($\geq$ 0.5–1 cm^{-3}) were not present. However, this does not rule out the possibility that fewer heterogeneous ice nuclei were present.

April 30, 1996 Case

The results of the simulation for the April 30 wave-cloud case are shown in Figure 3. In this simulation, the temperature is just high enough such that sulfate aerosols are activated into water droplets before the sulfate aerosols can freeze directly. Large numbers of liquid droplets are activated since there is no nucleation barrier to overcome. The liquid droplets grow, dilute, and freeze within 5–10 seconds. The droplets never get larger than about 1–2 μm radius. The peak ice crystal number density in the simulation (about 30 cm^{-3}) agrees well with the measurements for this case. The

Table 2. Wave-Cloud Sensitivity Tests (May 2 case)

#	Test	v_z	N_{cn}	N_{het}	σ_{cn}	N_{ice}	RHI$_{max}$
1	baseline	1.2	100	0	2.3	6.9	150.4
2	low v_z	0.8	100	0	2.3	4.0	149.0
3	high v_z	1.6	100	0	2.3	9.7	151.3
4	high N_{cn}	1.2	300	0	2.3	8.2	148.9
5	low N_{cn}	1.2	30	0	2.3	5.2	151.1
6	high σ_{cn}	1.2	100	0	2.8	6.1	149.1
7	low σ_{cn}	1.2	100	0	1.8	7.8	151.9
8[a]	low S_{crit}	1.2	100	0	2.3	17.0	126.6
9[a]	high S_{crit}	1.2	100	0	2.3	5.7	160.0
10[b]	slow grow	1.2	100	0	2.3	9.8	151.1
11	het. IN	1.2	100	0.1	2.3	6.3	149.9
12	het. IN	1.2	100	0.5	2.3	2.4	147.1
13	het. IN	1.2	100	0.7	2.3	0.71	140.7
14	het. IN	1.2	100	1	2.3	0.90	136.8
15	het. IN	1.2	100	2	2.3	1.8	131.7

The sensitivities of the peak ice crystal number densities, N_{ice} (cm^{-3}), and peak RHI (%) to updraft velocity, v_z (m-s^{-1}), sulfate aerosol number density, N_{cn} (cm^{-3}), heterogeneous freezing ice nuclei, N_{het} (cm^{-3}), and the width of the aerosol size distribution, σ_{cn}, are given.

[a]The aerosol freezing rate was increased (decreased) resulting in a decrease (increase) in the peak RHI.

[b]The deposition coefficient was decreased to 0.5, resulting in a 30% reduction in crystal growth rates.

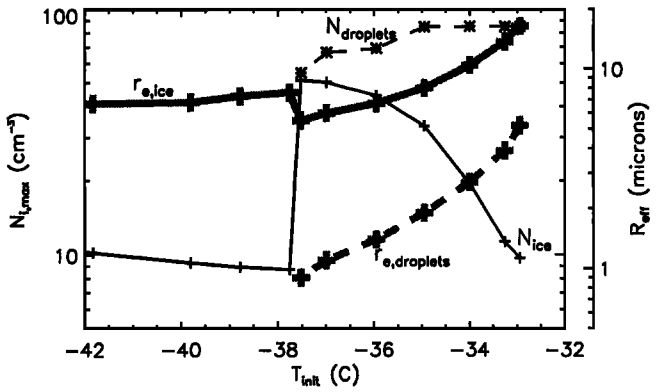

Figure 4. The peak liquid droplet and ice crystal number density are plotted versus minimum temperature for simulations with a range of initial temperatures. The effective radius of ice crystals in the simulations are also shown. The maximum number density of ice crystals forms at temperatures just low enough for liquid water droplets to form (near −37.5°C).

peak RHI in the simulation (147%) is somewhat larger than the observed peak values of about 135%; however, the locations where the peak RHIs occurred may not have been sampled on this flight.

The peak number of ice crystals is very sensitive to the formation of activated liquid droplets prior to ice nucleation in our simulations. Figure 4 shows the peak ice crystal and liquid droplet number densities versus the minimum temperature. If the temperature is just low enough such that the sulfate haze aerosols freeze before liquid drops form, then the peak ice number density should be less than 10 cm^{-3}; whereas the observations on April 30 showed ice number densities of 20–40 cm^{-3}.

The largest number of ice crystals is generated if the temperature is just cold enough such that liquid drops are activated. Above this temperature, the ice number density decreases with increasing temperature because the liquid droplets get larger before they freeze. Hence, when the first few droplets freeze, the resulting large ice crystals deplete the vapor rapidly, resulting in rapid evaporation of the remaining droplets before they can freeze. If the temperature drops just below −37.5°C such that the sulfate aerosols freeze before liquid droplets are activated, then the peak ice crystal number density drops dramatically. This lower number density results from the fact that the aerosol freezing rate is strongly dependent on their size and composition, and the freezing temperature varies substantially across the aerosol size range. Hence, the largest few aerosols freeze first, and the resulting crystals deplete the vapor before more aerosols can freeze.

The transition temperature of about −37.5°C predicted by our calculations is consistent with previous wave-cloud measurements [Heymsfield and Miloshevich, 1995]. Their measurements indicated droplets with radii up to a few μm in a cloud leading-edge with a temperature of −35°C. In a leading edge with a temperature of −37°C, droplets were marginally detectable with radii of only 1–2 μm. In a penetration at −44°C, no droplets formed. Also, the earlier wave-cloud measurements showed lower ice number densities (about 10 cm^{-3}) in the penetration at −44°C than in the warmer cases (about 20 cm^{-3}).

Heterogeneous freezing nuclei could potentially cause aerosol freezing before activation into droplets occurred, possibly resulting in a decrease in the ice crystal number density. If a very large fraction of the sulfate aerosols contained effective freezing nuclei, then the observed high ice number densities could have been generated without intermediate liquid droplet activation. However, given the high crystal number densities in this case, it seems likely that homogeneous freezing dominated the ice nucleation process.

Summary

Our model simulations including only homogeneous freezing nucleation predict peak humidities and ice number densities that agree with the SUCCESS wave-cloud observations (within the ranges of measurement and model uncertainties). The observations support the recent predictions that large supersaturations are required to initiate homogeneous freezing of sulfate aerosols. Sensitivity tests suggest that no more than about 0.5–1 cm^{-3} effective heterogeneous ice nuclei could have been present given the observed high supersaturations and ice number densities. We cannot rule out the possibility that smaller numbers of heterogeneous ice nuclei were present. In other types of cirrus clouds with lower cooling rates, small numbers of effective ice nuclei could dominate the ice nucleation process.

Acknowledgments. This research was supported by NASA's Subsonic Assessment Program, directed by Howard Wesoky.

References

Collins, J. E., et al., A novel external path water vapor sensor, presented at the Atmospheric Effects of Aviation Program 5th annual meeting, April 23–28, 1995.

Heymsfield, A. J., and R. M. Sabin, Cirrus crystal nucleation by homogeneous freezing of solution droplets, *J. Atmos. Sci., 46,* 2252, 1989.

Heymsfield, A. J., and L. M. Miloshevich, Homogeneous ice nucleation and supercooled liquid water in orographic wave clouds, *J. Atmos. Sci., 50,* 2335, 1993.

Heymsfield, A. J., and L. M. Miloshevich, Relative humidity and temperature influences on cirrus formation and evolution: Observations from wave clouds and FIRE II, *J. Atmos. Sci., 52,* 4302, 1995.

Jensen, E. J., et al., Microphysical modeling of cirrus part I: Comparison with 1986 FIRE IFO measurements, J. Geophys. Res., , *99,* 10421, 1994.

Jensen, E. J., and O. B. Toon, Ice nucleation in the upper troposphere: Sensitivity to aerosol number density, temperature, and cooling rate, Geophys. Res. Lett., , *21,* 2019, 1994.

Jensen, E. J., and O. B. Toon, The potential impact of soot particles from aircraft exhaust on cirrus clouds, Geophys. Res. Lett., , *24,* 249, 1997.

Liou, K.-N., S. C. Ou, and C. Koenig, An investigation on the climatic effect of contrail cirrus, Lecture Notes in Engrg., Vol. 60, Springer, Berlin, 138-153, 1990.

Sassen, K., et al., Mesoscale and microscale structure of cirrus clouds: Three case studies, *J. Atmos. Sci., 46,* 371, 1989.

Sassen, K., and G. C. Dodd, Haze particle nucleation simulations in cirrus clouds, and applications for numerical and lidar studies, *J. Atmos. Sci., 46,* 3005–3014, 1989.

Tabazadeh, A., E. Jensen, and O. B. Toon, A model description for cirrus cloud nucleation from homogeneous freezing of sulfate aerosols, submitted to *J. Geophys. Res.*, 1997.

Eric. J. Jensen, NASA Ames Research Center, MS 245-4, Moffett Field, CA 94035.

(Received June 25, 1997; revised November 20, 1997; accepted November 25, 1997.)